Editors' Suggestion

Photon-Mediated Spin-Exchange Dynamics of Spin-1 Atoms

Emily J. Davis, Gregory Bentsen, Lukas Homeier, Tracy Li, and Monika H. Schleier-Smith
Department of Physics, Stanford University, Stanford, California 94305, USA

(Received 6 September 2018; published 9 January 2019)

We report direct observations of photon-mediated spin-exchange interactions in an atomic ensemble. Interactions extending over a distance of 500 μm are generated within a cloud of cold rubidium atoms coupled to a single mode of light in an optical resonator. We characterize the system via quench dynamics and imaging of the local magnetization, verifying the coherence of the interactions and demonstrating optical control of their strength and sign. Furthermore, by initializing the spin-1 system in the $m_f = 0$ Zeeman state, we observe correlated pair creation in the $m_f = \pm 1$ states, a process analogous to spontaneous parametric down-conversion and to spin mixing in Bose-Einstein condensates. Our work opens new opportunities in quantum simulation with long-range interactions and in entanglement-enhanced metrology.

DOI: 10.1103/PhysRevLett.122.010405

The hallmark of quantum information is its capacity to be nonlocal, encoded in correlations among entangled particles. By contrast, the interactions between particles are necessarily local, restricting the quantum states that arise in nature. Nevertheless, nonlocal interactions appear in a wide range of conceptual models, from holographic models of quantum gravity [1] to spin models encoding hard optimization problems [2,3] that are intimately connected to the physics of spin glasses [4,5].

Effectively nonlocal models can be generated in the laboratory by coupling atoms or solid-state qubits to optical or microwave resonators, where photons mediate long-range interactions [6–15]. In atomic ensembles, interfacing photons with collective motional degrees of freedom has led to remarkable self-organization phenomena [11–16] including supersolidity [13], while photon-mediated spin interactions [17–19] have been harnessed to prepare squeezed states [8,9] for quantum metrology.

Past experiments realizing cavity-mediated spin interactions have focused on manipulating and probing collective degrees of freedom [8–10,14–16]. For example, for atoms initialized in a spin-polarized state and uniformly coupled to a single cavity mode, the subsequent dynamics can be completely characterized by inferring moments of the total magnetization from measurements of the outgoing light. In principle, photon-mediated interactions can also access richer many-body physics [4,5,20–22], including topological phases of matter [23,24] and dynamical gauge fields [25,26]. However, fully benefiting from the nonlocal character of the interactions requires combining strong atom-light coupling with local addressing and imaging of spin dynamics.

Of particular interest for prospective applications in quantum simulation [20,21,23] are light-induced spin-exchange interactions. Several theoretical proposals envision tuning the strength, sign, or spatial structure of spin-exchange couplings via optical drive fields [20,21,23]. While spin-exchange interactions mediated by the vacuum field in a cavity [10,27,28] have recently been detected [10], achieving optical control over similar interactions requires a two-photon coupling between spin states, e.g., hyperfine or Zeeman states. The latter encoding furthermore enables exploration of higher-spin models, including long-range-interacting analogs of spinor Bose condensates [29–35].

In this Letter, we report direct observations of photon-mediated spin-exchange interactions in an ensemble of spin-1 atoms. Spin excitations generated in one region of a spatially extended atomic cloud are observed to hop coherently over a distance of hundreds of microns. We characterize the interactions via quench dynamics, demonstrating optical control of the interactions' strength and sign. Furthermore, for a system initialized in the $m_f = 0$ Zeeman state, we observe light-mediated spin mixing, evidenced by correlated population growth in the $m_f = \pm 1$ states. An analog of spontaneous parametric down-conversion, this pair creation process paves the way to generating new many-atom entangled states.

The scheme for generating spin-exchange interactions is illustrated in Fig. 1. The building block is a Raman process in which an atom changes its internal state by absorbing a photon from a control field and emitting it into a cavity mode. When the Raman coupling is resonant, its dominant effect is to induce superradiant decay [36]. For a control field detuned from Raman resonance, however, virtual emission into the cavity can induce a "flip-flop" process, wherein a second atom flips its spin by absorbing the virtual photon and rescattering it into the mode of the control field.

The flip-flop dynamics are described by an effective Hamiltonian [37]

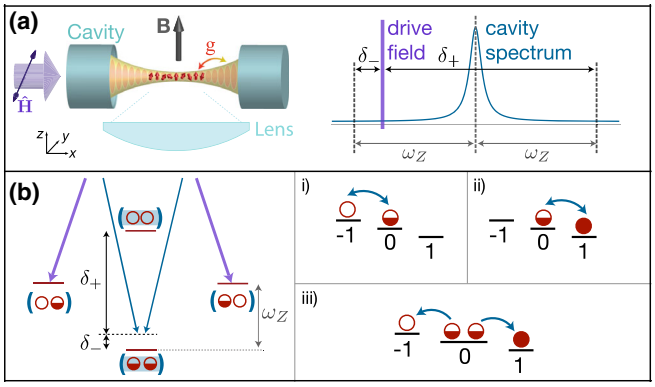

FIG. 1. Experimental setup and scheme for generating spin-exchange interactions. (a) Driven cavity with atoms (red), transverse magnetic field, and imaging lens. The drive field is detuned by $\delta_\pm$ from Raman resonances. (b) Pairwise interactions are generated by one atom scattering a photon from the driven cavity mode (purple) into the orthogonally polarized cavity mode (blue), and a second atom rescattering the photon. This mechanism can produce spin-exchange interactions (i),(ii) or spin mixing (iii). Red circles indicate spin states $m = -1$ (empty), $m = 0$ (half-filled), and $m = 1$ (full).

$$H = \hbar \sum_{i,j} (\chi_{ij}^{+} f_i^{+} f_j^{-} + \chi_{ij}^{-} f_i^{-} f_j^{+}), \tag{1}$$

where $\mathbf{f}_i$ denote the spins of individual atoms, each pinned to a fixed location. The strengths of the spin-exchange couplings $\chi_{ij}^{\pm}$ are controlled by the amplitude of a drive field, as well as the spatial profile of the cavity mode. The sign of the interactions is governed by the detunings $\delta_\pm$ from two Raman resonances, illustrated in Fig. 1. Hence, the interactions can be ferromagnetic or antiferromagnetic depending on the frequency of the control field.

To understand the dynamics that we expect to observe, we may view each spin-1 atom as a site that can hold up to two spin excitations. The flip-flop process then corresponds to hopping of a spin excitation between two sites [Fig. 1(b)], mediated by converting the spin excitation into an intracavity photon. Besides exchanging empty and singly occupied (or singly and doubly occupied) sites at arbitrary distances, this process can transform two singly occupied sites into a doublon-hole pair. We will be able to observe either of these processes—spin exchange or pair creation—depending how we initialize the system.

We investigate the spin dynamics in a cloud of $N \sim 10^5$ rubidium-87 atoms trapped in a standing wave of 1560-nm light in a single-mode optical resonator. The conduit for mediating interactions is a 780-nm cavity mode at large detuning $\Delta = -2\pi \times 10$ GHz from the $|5S_{1/2}, f = 1\rangle \rightarrow |5P_{3/2}\rangle$ transitions. The coherence of the atom-light coupling at cavity center, where the mode has a 16-μm waist, is parametrized by the single-atom cooperativity $\eta \equiv 4g^2/(\kappa\Gamma) = 7.5$. Here, $2g = 2\pi \times 3.0(2)$ MHz is the vacuum Rabi frequency, $\Gamma = 2\pi \times 6$ MHz is the atomic excited-state linewidth, and $\kappa = 2\pi \times 200(50)$ kHz is the cavity linewidth.

The scheme for inducing spin-exchange interactions [Fig. 1(b)] can be implemented either by directly driving the atoms or by driving the cavity. We adopt the latter approach. The atoms are initialized in the $f = 1$ hyperfine manifold, and we apply a uniform magnetic field $B\hat{z}$ transverse to the cavity axis [Fig. 1(a)] to produce a Zeeman splitting $\omega_Z = \mu_B B/2$. Spins placed in a superposition of Zeeman levels then undergo a Larmor precession that couples to the cavity via the Faraday effect, introducing a modulated birefringence. For a cavity driven with horizontal ($\hat{\mathbf{H}}$) polarization, the atoms thus modulate the polarization of the intracavity field—or, equivalently, scatter photons from the $\hat{\mathbf{H}}$-polarized into the $\hat{\mathbf{V}}$-polarized cavity mode. These scattered photons mediate the interactions among the spins.

To generate coherent interactions, we drive the cavity with a control field detuned from Raman resonance. Letting ω_c^N denote the cavity resonance frequency in the presence of the atoms, tuning the drive field to a frequency $\omega_d = \omega_c^N + \delta_c$ results in detunings $\delta_\pm = \delta_c \mp \omega_Z$ from the two Raman resonances shown in Fig. 1. While driving on either resonance ($\delta_\pm = 0$) produces superradiant decay, with increasing detuning $\delta_\pm > \kappa$ we expect the decay to be suppressed relative to coherent interactions induced by the back-action of the cavity field on the atoms [37].

To observe the photon-mediated interactions (Fig. 2), we first initialize all atoms in $|m_f = -1\rangle$ in a 4 G magnetic field. We apply a local Raman $\pi/2$ pulse to populate a region of the cloud (A) with spin excitations. At time $t = 0$, we switch on the cavity drive field at a detuning $\delta_- = 2\pi \times 1.7$ MHz. We observe the subsequent evolution of the spins by state-sensitive imaging [37]. We regard the system as one-dimensional, integrating over the transverse

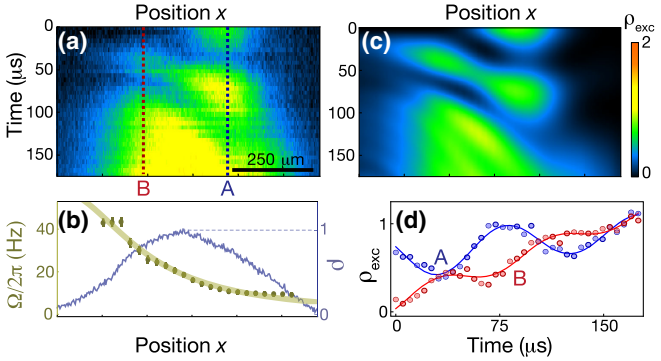

FIG. 2. Cavity-mediated spin-exchange interactions. (a) Driving the cavity induces spin excitations to hop from the right side of the atomic cloud (A) to the left (e.g., B) and back. The vector light shift $\Omega(x)$ (b) (yellow) and atomic density profile $\rho(x)$ (b) (blue) serve as input to a mean-field model (c) of the spin dynamics. (d) Oscillations in excitation density ρ_{exc} vs time along cuts A and B; lines are guides to the eye.

dimensions of the atomic cloud and plotting the local density of spin excitations $\rho_{\mathrm{exc}} = \rho[1 + \langle f^z \rangle]$ vs time, where $\langle \mathbf{f} \rangle$ is the local spin polarization and ρ is the local atomic density, normalized to peak density. The data show a coherent oscillation of spin excitations from the initially populated region (A) to elsewhere in the cloud (B) and back [Figs. 2(a) and 2(d)].

A striking feature of the spin dynamics is their highly nonlocal character. The spin excitations first hop towards the left edge of the cloud, rather than to regions closer to the initially excited area [Fig. 2(a)]. More generally, we observe a spatial gradient in the timescale of the spin dynamics, which we attribute to a gradient in atom-light coupling: the coupling is strongest at the left because the atoms are displaced from the cavity center.

To verify our understanding of the atom-light interactions, we have directly measured the ac Stark shift induced by the intracavity light as a function of position x along the cavity axis. Figure 2(b) shows the on-axis vector light shift $\Omega(x) = [g^2_{m=-1}(x) - g^2_{m=1}(x)]/(2\Delta)$ per circularly polarized intracavity photon. The light shifts $\Omega_i \equiv \Omega(x_i)$ determine the spin-exchange couplings $\chi^{\pm}_{ij} = \bar{n}\Omega_i\Omega_j\mathcal{A}(\delta_{\pm})/\kappa$, where $\bar{n}$ is the average intracavity photon number and $\mathcal{A}(\delta) = \delta\kappa/\{16[\delta^2 + (\kappa/2)^2]\}$ [37].

We use the measured light shift as input to a mean-field model [Fig. 2(c)] with which we compare the observed spin dynamics. By reproducing the spatial structure of oscillations in the magnetization, the model corroborates the graph of nonlocal interactions $\chi^{\pm}_{ij}$. The model also captures two dissipation mechanisms observed in the experiment: cavity decay induces spin relaxation towards $m_F = 1$, while inhomogeneous broadening due to the 5 μm rms transverse cloud size causes additional damping [37].

The effects of cavity decay visible in Fig. 2(a) can theoretically be reduced by increasing the detuning $\delta_{\pm}$ from Raman resonance. An optimal detuning $\delta_{\mathrm{opt}} \sim \sqrt{N\eta}\kappa$ is dictated by the collective cooperativity $N\eta = 4Ng^2/(\kappa\Gamma) \sim 10^6$, which quantifies two competing decay channels: collective decay via the cavity at small $\delta_{\pm}$ and spontaneous emission at larger $\delta_{\pm}$, where a stronger control field is required to maintain a fixed interaction strength. Finite laser power currently limits us to small detunings $\delta_{\pm} \ll \delta_{\mathrm{opt}}$, leaving room to improve the interaction-to-decay ratio by a factor of 10^2 in future experiments [37].

Both the overall strength of the interactions and their sign are controlled by the drive laser. However, the hopping dynamics of Fig. 2 do not reveal the sign of the couplings χ_{ij}. To more fully characterize the interactions, we note that the spin-exchange Hamiltonian can equivalently be rewritten as

$$H = \sum_{i,j} \chi_{ij}(f^x_i f^x_j + f^y_i f^y_j) + \sum_i h_i f^z_i, \qquad (2)$$

where we have set $\hbar = 1$. Here $\chi_{ij} = \chi^{+}_{ij} + \chi^{-}_{ij}$, and $h_i = \chi^{+}_{ii} - \chi^{-}_{ii}$. By Eq. (2), each spin precesses about an effective field in the xy plane generated by all other spins. The rate and direction of the spin precession then reveal the magnitude and sign of χ_{ij}.

To measure the couplings χ_{ij}, we first prepare the noninteracting system with a spin texture in the $\hat{f}_x$, $\hat{f}_y$ plane [Fig. 3(a.i)]. Using a pair of Raman pulses, we initialize one portion of the cloud [centered about region A in Fig. 3(a)] with spins polarized along $\hat{f}_x$ and the remainder of the cloud (centered about region B) with spins polarized along $\hat{f}_y$, where the axes $\hat{f}_{x,y}$ are defined in a rotating frame at the Larmor frequency. By Eq. (2), cavity-mediated interactions should induce the $\hat{f}_x$- and $\hat{f}_y$-polarized spins to precess about one another in a direction that depends on the sign of χ_{ij} [Fig. 3(a.ii)]. This precession converts the transverse spin texture into a signal in the longitudinal polarization $\langle f^z \rangle$.

The magnetization dynamics allow us to measure both the strength and sign of the flip-flop coupling as a function of drive frequency. For ideal unitary dynamics, the initial rate of change df^z_i/dt of each atom's magnetization would reveal its total coupling $\chi_i = \sum_j \chi_{ij}$ to all other spins. By comparing the initial slopes $\langle df^z/dt \rangle_{A,B}$ in regions A and B, and accounting for the calibrated spatial dependence of the atom-light coupling $\Omega(x)$, we extract both the mean spin relaxation rate $\langle \gamma_i \rangle$ and mean total coupling $\langle \chi_i \rangle$ within each region.

Figure 3(b) compares the measured flip-flop coupling with theory. Consistent with our expectation, the sign of the interaction changes as the drive frequency crosses through

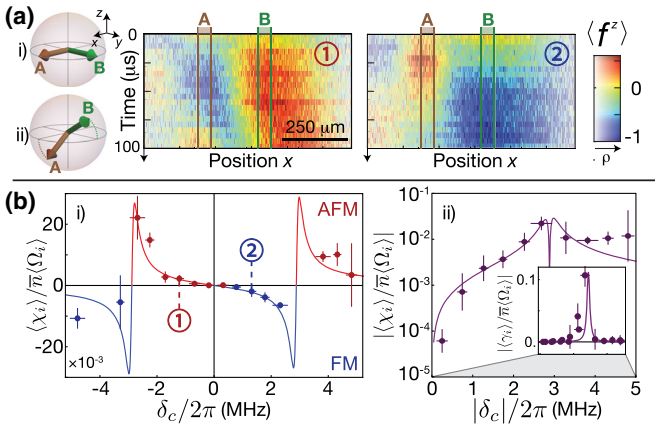

FIG. 3. Optical control of spin-exchange interactions. (a) Spins in regions A and B are initially oriented along $\hat{f}_x$ and $\hat{f}_y$, respectively. Light-induced interactions convert this transverse polarization into a signal in $\langle f^z \rangle$, shown for two different drive frequencies. Color scale indicates $\langle f^z \rangle$ (hue) and density ρ (saturation). (b) Varying the drive frequency changes the sign of interactions from antiferromagnetic (red) to ferromagnetic (blue). Solid curve is a fit with amplitude as the only free parameter. Right plot (ii) shows agreement of interaction strength $|\langle \chi_i \rangle|$ with theory across 2 orders of magnitude. Inset shows spin relaxation rate $\langle \gamma_i \rangle$.

each of the Raman resonances $\delta_c = \pm\omega_Z$, and at the cavity resonance $\delta_c = 0$, where $\chi_{ij}^{+} = -\chi_{ij}^{-}$. This change in sign is evident in a striking reversal of the slopes of the magnetization vs time in regions A and B of the cloud. The interaction strength per intracavity photon agrees with the independently calibrated atom-cavity coupling and also follows the predicted dependence on detuning over a wide dynamic range [Fig. 3(b.ii)]. Lastly, the magnetization data confirm that the dissipation $\langle\gamma_i\rangle$ is highest on two-photon resonance ($\delta_c = \pm\omega_Z$).

Whereas the spin-exchange dynamics considered above can be understood by regarding the spins as precessing about a classical mean field $\langle\mathbf{f}\rangle$, the quantum system can exhibit dynamics even with zero average magnetization $\langle\mathbf{f}\rangle = 0$. To access dynamics driven by quantum fluctuations, we initialize an ensemble of atoms in $|m_f = 0\rangle$, which the flip-flop interactions can convert into correlated pairs of atoms in $|m_f = \pm 1\rangle$ [Fig. 1(b.iii)]. This spin mixing process is analogous to an optical parametric oscillator, with the large population N_0 of $|m_f = 0\rangle$ atoms serving as a pump.

The spin mixing can thus be understood by viewing the atomic populations in $m_f = \pm 1, 0$ as excitations of three bosonic modes a, b, c. In the limit of uniform coupling $\chi_{ij} \sim \chi$, we can rewrite the spin operators in Eq. (1) in terms of these modes:

$$H_{\mathrm{mix}} = 2\chi c^2 a^\dagger b^\dagger + \mathrm{H.c.} + H_q, \tag{3}$$

where the first term is responsible for pair creation and $H_q = (2\chi c^\dagger c + q + \chi)(a^\dagger a + b^\dagger b + 1)$ includes a quadratic Zeeman shift $q/B^2 = 2\pi \times 144\ \mathrm{Hz/G^2}$ that can suppress pair creation. Instability to the production of pairs occurs when the collective interaction strength $4N_0\chi$ is larger in magnitude than the quadratic Zeeman shift and has opposite sign [37], as observed in ferromagnetic spinor condensates [31,32,35,43,44].

To enable cavity-mediated pair creation, we initialize nearly all atoms in $|m_f = 0\rangle$ in a weak magnetic field $B = 1.14$ G and induce ferromagnetic interactions with a red-detuned drive field. After driving the cavity at Raman detuning $\delta_- = -2\pi \times 600$ kHz for a variable time $t \leq 1.2$ ms, we image the populations of the three Zeeman states. Figure 4(a) shows representative images from 40 iterations of such an experiment, with $t = 400$ μs. We observe a macroscopic population of the $m_f = \pm 1$ "side modes" (Fig. 4), with large shot-to-shot fluctuations that are well correlated between the $m_f = \pm 1$ states.

The rapid growth in total side mode population N_s at fixed population difference $F_z = a^\dagger a - b^\dagger b$ is qualitatively consistent with the parametric amplification model H_{mix}. In the experimentally relevant limit $|\chi| \ll q \ll N_0|\chi|$, this model predicts an initial population growth

$$N_s(t) = \left[\frac{4N_0\chi}{\lambda}\right]^2 [N_s(0) + 1](\cosh\lambda t - 1) + N_s(0), \tag{4}$$

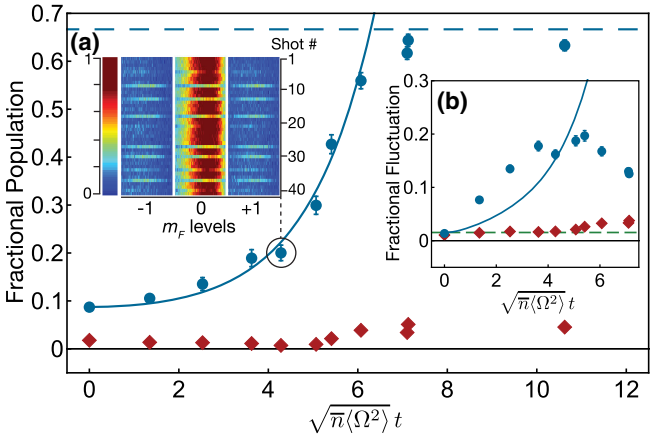

FIG. 4. Cavity-mediated spin mixing in a cloud of $N = 10^5$ atoms. (a) Average side mode population N_s (blue circles) and population difference F_z (red diamonds) vs $\sqrt{\bar{n}\langle\Omega^2\rangle}t$ [37], measured for interaction times $0 \leq t \leq 1.2$ ms with typical intracavity photon number $\bar{n} \approx 3 \times 10^3$. Inset: images from 40 iterations of the experiment with $t = 400$ μs; colors indicate fractional population in each state. (b) Fluctuations in side mode population ΔN_s (blue circles) and population difference ΔF_z (red diamonds). Solid blue curves are obtained by fitting N_s with the model in Eq. (4) and plotting the corresponding prediction for ΔN_s with no free parameters. Dashed blue line in (a) indicates saturation level $N_s/N = 2/3$ for the side mode population. Dashed green line in (b) indicates detection noise.

where $\lambda = 4\sqrt{N_0 q|\chi|}$ and $N_s(0)$ represents initial population in the side modes, present in the experiment due to imperfect state preparation. Fitting Eq. (4) to the early-time population dynamics in the experiment (Fig. 4, solid blue) yields a time constant $1/\lambda = 160(20)$ μs for the exponential growth, which is 6 times slower than expected for a system with uniform coupling equal to the rms coupling $\sqrt{\langle\Omega^2\rangle}$ in our system. The slower growth we observe may be due to additional effects of inhomogeneity or residual population in hyperfine states not included in the three-mode model.

The parametric amplification model predicts macroscopic fluctuations in side mode population, with $\Delta N_s \approx N_s/\sqrt{2}$ at early times. While the overall scale of the fluctuations that we observe roughly matches this expectation [Fig. 4(b)], a more detailed analysis remains a subject for future investigation. Of particular interest are the fluctuations in population difference F_z, which for ideal unitary pair creation should remain zero. The measured fluctuations in F_z at short times are currently dominated by percent-level technical noise in state preparation and detection [Fig. 4(b), dashed green line]. Reducing this technical noise—or harnessing interaction-based readout [9,43,45]—will allow for probing entanglement between the $m_f = \pm 1$ modes [46], enabling applications in quantum metrology [29].

Notably, light-mediated spin mixing will allow for generating spin nematic squeezing and twin Fock states

significantly faster than in past experiments harnessing contact interactions [29–35]. The optically controlled interactions further allow for probing ferromagnetic and antiferromagnetic spinor phases in a single atomic species, and for tuning the interaction range [23].

The combination of nonlocal spin interactions with local addressing and imaging opens the door to controlling and probing the spatial structure of entanglement. Applications range from quantum-enhanced magnetic field imaging to investigating fundamental limits on the propagation of quantum correlations [47]. Quantum optical approaches to combinatorial optimization problems [5,48], e.g., number partitioning [2,3], could be explored by positioning individual spins to specify their interactions. Extensions of our scheme will allow for engineering a wider range of nonlocal graphs [23], enabling exotic long-range interactions that can stabilize topological order [23] or mimic toy models of quantum gravity [49].

This work was supported by the National Science Foundation under Grant No. PHY-1506401 and by the Research Corporation Cottrell Scholars Program. E. J. D. and G. B. acknowledge support from the National Science Foundation Graduate Research Fellowship Program. E. J. D. acknowledges support from the Hertz Foundation. L. H. acknowledges support from the Max Weber Foundation. T. L. was supported by the Air Force Office of Scientific Research. We thank R. Yanagimoto for technical assistance.

[1] S. Sachdev, Phys. Rev. X **5**, 041025 (2015).
[2] A. Lucas, Frontiers Phys. **2**, 5 (2014).
[3] S. Mertens, Phys. Rev. Lett. **81**, 4281 (1998).
[4] P. Strack and S. Sachdev, Phys. Rev. Lett. **107**, 277202 (2011).
[5] S. Gopalakrishnan, B. L. Lev, and P. M. Goldbart, Phys. Rev. Lett. **107**, 277201 (2011).
[6] J. Majer, J. Chow, J. Gambetta, J. Koch, B. Johnson, J. Schreier, L. Frunzio, D. Schuster, A. Houck, A. Wallraff, A. Blais, M. Devoret, S. Girvin, and R. Schoelkopf, Nature (London) **449**, 443 (2007).
[7] A. F. Van Loo, A. Fedorov, K. Lalumière, B. C. Sanders, A. Blais, and A. Wallraff, Science **342**, 1494 (2013).
[8] I. D. Leroux, M. H. Schleier-Smith, and V. Vuletić, Phys. Rev. Lett. **104**, 073602 (2010).
[9] O. Hosten, R. Krishnakumar, N. Engelsen, and M. Kasevich, Science **352**, 1552 (2016).
[10] M. A. Norcia, R. J. Lewis-Swan, J. R. Cline, B. Zhu, A. M. Rey, and J. K. Thompson, Science **361**, 259 (2018).
[11] A. T. Black, H. W. Chan, and V. Vuletić, Phys. Rev. Lett. **91**, 203001 (2003).
[12] A. J. Kollár, A. T. Papageorge, V. D. Vaidya, Y. Guo, J. Keeling, and B. L. Lev, Nat. Commun. **8**, 14386 (2017).
[13] J. Léonard, A. Morales, P. Zupancic, T. Esslinger, and T. Donner, Nature (London) **543**, 87 (2017).
[14] M. Landini, N. Dogra, K. Kroeger, L. Hruby, T. Donner, and T. Esslinger, Phys. Rev. Lett. **120**, 223602 (2018).
[15] R. M. Kroeze, Y. Guo, V. D. Vaidya, J. Keeling, and B. L. Lev, Phys. Rev. Lett. **121**, 163601 (2018).
[16] Z. Zhiqiang, C. H. Lee, R. Kumar, K. Arnold, S. J. Masson, A. Parkins, and M. Barrett, Optica **4**, 424 (2017).
[17] A. André, L.-M. Duan, and M. D. Lukin, Phys. Rev. Lett. **88**, 243602 (2002).
[18] A. Sondberg Sørensen and K. Mølmer, Phys. Rev. A **66**, 022314 (2002).
[19] M. H. Schleier-Smith, I. D. Leroux, and V. Vuletić, Phys. Rev. A **81**, 021804 (2010).
[20] B. Swingle, G. Bentsen, M. Schleier-Smith, and P. Hayden, Phys. Rev. A **94**, 040302 (2016).
[21] E. Colella, R. Citro, M. Barsanti, D. Rossini, and M.-L. Chiofalo, Phys. Rev. B **97**, 134502 (2018).
[22] F. Mivehvar, F. Piazza, and H. Ritsch, Phys. Rev. Lett. **119**, 063602 (2017).
[23] C.-L. Hung, A. González-Tudela, J. I. Cirac, and H. Kimble, Proc. Natl. Acad. Sci. U.S.A. **113**, E4946 (2016).
[24] F. Mivehvar, H. Ritsch, and F. Piazza, Phys. Rev. Lett. **118**, 073602 (2017).
[25] W. Zheng and N. R. Cooper, Phys. Rev. Lett. **117**, 175302 (2016).
[26] K. E. Ballantine, B. L. Lev, and J. Keeling, Phys. Rev. Lett. **118**, 045302 (2017).
[27] J. Hu, W. Chen, Z. Vendeiro, A. Urvoy, B. Braverman, and V. Vuletić, Phys. Rev. A **96**, 050301 (2017).
[28] R. J. Lewis-Swan, M. A. Norcia, J. R. K. Cline, J. K. Thompson, and A. M. Rey, Phys. Rev. Lett. **121**, 070403 (2018).
[29] S. J. Masson, M. D. Barrett, and S. Parkins, Phys. Rev. Lett. **119**, 213601 (2017).
[30] M.-S. Chang, Q. Qin, W. Zhang, L. You, and M. S. Chapman, Nat. Phys. **1**, 111 (2005).
[31] L. Sadler, J. Higbie, S. Leslie, M. Vengalattore, and D. Stamper-Kurn, Nature (London) **443**, 312 (2006).
[32] C. Klempt, O. Topic, G. Gebreyesus, M. Scherer, T. Henninger, P. Hyllus, W. Ertmer, L. Santos, and J. J. Arlt, Phys. Rev. Lett. **104**, 195303 (2010).
[33] B. Lücke, M. Scherer, J. Kruse, L. Pezzé, F. Deuretzbacher, P. Hyllus, J. Peise, W. Ertmer, J. Arlt, L. Santos *et al.*, Science **334**, 773 (2011).
[34] C. D. Hamley, C. Gerving, T. Hoang, E. Bookjans, and M. S. Chapman, Nat. Phys. **8**, 305 (2012).
[35] X.-Y. Luo, Y.-Q. Zou, L.-N. Wu, Q. Liu, M.-F. Han, M. K. Tey, and L. You, Science **355**, 620 (2017).
[36] J. Kohler, J. A. Gerber, E. Dowd, and D. M. Stamper-Kurn, Phys. Rev. Lett. **120**, 013601 (2018).
[37] See Supplemental Material at http://link.aps.org/supplemental/10.1103/PhysRevLett.122.010405 for supporting derivations and additional experimental details, including Refs. [38–42].
[38] K. Hammerer, A. S. Sørensen, and E. S. Polzik, Rev. Mod. Phys. **82**, 1041 (2010).
[39] F. Reiter and A. S. Sørensen, Phys. Rev. A **85**, 032111 (2012).
[40] B. Yurke, S. L. McCall, and J. R. Klauder, Phys. Rev. A **33**, 4033 (1986).

[41] K. Wodkiewicz and J. H. Eberly, J. Opt. Soc. Am. B **2**, 458 (1985).
[42] C. C. Gerry, Phys. Rev. A **31**, 2721 (1985).
[43] D. Linnemann, H. Strobel, W. Muessel, J. Schulz, R. J. Lewis-Swan, K. V. Kheruntsyan, and M. K. Oberthaler, Phys. Rev. Lett. **117**, 013001 (2016).
[44] D. M. Stamper-Kurn and M. Ueda, Rev. Mod. Phys. **85**, 1191 (2013).
[45] E. Davis, G. Bentsen, and M. Schleier-Smith, Phys. Rev. Lett. **116**, 053601 (2016).
[46] B. Lücke, J. Peise, G. Vitagliano, J. Arlt, L. Santos, G. Tóth, and C. Klempt, Phys. Rev. Lett. **112**, 155304 (2014).
[47] G. Bentsen, Y. Gu, and A. Lucas, arXiv:1805.08215.
[48] V. Torggler, P. Aumann, H. Ritsch, and W. Lechner, arXiv:1803.00735.
[49] S. S. Gubser, J. Knaute, S. Parikh, A. Samberg, and P. Witaszczyk, Commun. Math. Phys. **352**, 1019 (2017); S. S. Gubser, C. Jepsen, Z. Ji, and B. Trundy, Phys. Rev. D **98**, 045009 (2018).